Leptonic signatures of color-sextet scalars. II. Exploiting unique large-$E_{\mathrm{T}}^{\mathrm{miss}}$ signals at the LHC

Linda M. Carpenter* and Katherine Schwind†

Department of Physics, The Ohio State University, 191 W. Woodruff Avenue, Columbus, Ohio 43210, USA

Taylor Murphy‡

Laboratoire de Physique Théorique et Hautes Énergies (LPTHE), UMR 7589, Sorbonne Université and CNRS, 4 place Jussieu, 75252 Paris Cedex 05, France

(Received 4 January 2024; accepted 26 February 2024; published 8 April 2024)

The diverse and distinct collider phenomenology of color-sextet scalars motivates a thorough investigation of their effective couplings to the Standard Model at the LHC. Some of the more unique sextet signals involve not only jets but also leptons. In previous work, we proposed an LHC search for color-sextet scalars in a channel with jets and a hard opposite-sign lepton pair, which results from a dimension-six coupling. In this sequel we study the counterpart processes with neutrinos, which produce jets in association with missing transverse energy ($E_{\mathrm{T}}^{\mathrm{miss}}$) in addition to possible leptons. We consider multiple search channels, including both single and pair sextet production, all characterized by significant missing energy and some featuring distinctive kinematic features. Our multifaceted study consists of three reinterpreted existing searches and a joint-likelihood analysis designed by us to maximize HL-LHC sensitivity to single sextet production. We show that our dedicated strategy in the jets + lepton + $E_{\mathrm{T}}^{\mathrm{miss}}$ channel can supersede today's limits from reinterpreted searches, and we make sensitivity projections for the HL-LHC. Altogether, our analysis can exclude sextet scalars lighter than 4.4 TeV or probe effective cutoffs as high as 16.8 TeV.

DOI: 10.1103/PhysRevD.109.075010

I. INTRODUCTION

As Run 3 of the Large Hadron Collider (LHC) gets underway, the high-energy physics community has an opportunity to assess the strategies it has employed in the ongoing search for physics beyond the Standard Model (bSM), with an eye toward maximizing the LHC's utility in the next decade and beyond. This assessment must be conducted in view of not only the improving performance and increasingly large dataset of the LHC, but also the lack of definitive evidence for bSM physics produced by LHC Runs 1 and 2. The latter reality has already been driving a shift during the past few years from the traditional focus on elaborate constructions featuring, e.g., supersymmetry to more broadly applicable frameworks, exemplified by simplified models and effective field theories (EFTs). Indeed a broader approach seems appropriate in the absence of any specific experimental hints, and given the simple fact that much of the enormous bSM parameter space still has yet to be investigated. Models featuring new states in exotic representations of the SM color gauge group(s), $\mathrm{SU}(3)_{\mathrm{c}}$, are particularly ripe for investigation at hadron colliders.

Color sextets, which transform in the six-dimensional irreducible representation (**6**) of $\mathrm{SU}(3)_{\mathrm{c}}$, were first studied a few decades ago [1,2] and have garnered some renewed interest in the twenty-first century. Many works have focused on *sextet diquarks* [3], scalars so named for their renormalizable couplings to like-sign pairs of right-chiral ("handed") SM quarks of the form

$$\mathcal{L} \propto K_s{}^{ij}\Phi^{\dagger s}\overline{q_{\mathrm{R}i}^{\mathrm{c}}}q'_{\mathrm{R}j} + \mathrm{H.c.}, \tag{1}$$

where $K_s{}^{ij}$ ($s \in \{1,\ldots,6\}$) are $(i \leftrightarrow j)$-symmetric coefficients in color space, and where $q, q' \in \{u, d\}$ pursuant to the weak hypercharge of the sextet diquark Φ. Some of the LHC phenomenology of these particles has been studied both in a standalone context [4,5] and embedded as messengers between the Standard Model and fermionic dark matter [6]. While the number of gauge-invariant renormalizable sextet-SM interactions is small (though even these are rich and worth further attention), there

*lmc@physics.osu.edu
†schwind.44@osu.edu
‡murphy@lpthe.jussieu.fr

are a large number of effective interactions at relatively low mass dimensions that have just begun to be studied [7]. Effective operators that integrate out some ultraviolet degrees of freedom but retain sextets at the weak or TeV scale themselves constitute but one subclass of a huge collection of operators with light exotics that offer alternative paths to discovery of bSM physics at the LHC [8].

In this spirit, we recently undertook an effort to identify and analyze the LHC signatures of exotic effective operators containing color-sextet scalars, beginning with a proposal to search for sextets produced in association with electrons or muons [9]. There we targeted events featuring at least two hard jets and an opposite-sign lepton pair, which are generated by a dimension-six coupling between a color-sextet scalar, the SM gluon, and a right-handed quark-lepton pair. Excellent sensitivity can be achieved at the LHC by binning the invariant mass of the scalar's decay products: in particular, a search along the lines of what we proposed in that work can probe sextet masses up to $m_\Phi = 5$ TeV, or effective cutoff scales Λ of $\mathcal{O}(10)$ TeV, with the planned $\mathcal{L} = 3$ ab^{-1} run of the High-Luminosity (HL-)LHC.

The present work is a natural extension of that study: it targets that operator's left-handed counterpart, which couples a color-sextet scalar to the SM quark/lepton weak doublets. This operator, in addition to producing sextet-lepton(-quark-gluon) couplings, permits the scalar to interact with a SM neutrino. These couplings open multiple interesting production and decay channels that will produce events with significant missing energy and distinct kinematics at the LHC. Since the sextet can be both pair produced and singly produced in association with a charged lepton or neutrino—and then decay to either as well—we consider all possibilities in order to achieve the best possible sensitivity for the full planned run of the HL-LHC.

Our multifaceted analysis is centered on a joint-likelihood analysis in a single-production channel we call "mostly visible," which includes one charged lepton from either production (i.e., recoiling off of the sextet scalar) or decay. We design a search strategy for this channel and compute a joint likelihood based on a binned distribution of $m_{\mathrm{T}}(j_1 j_2, E_{\mathrm{T}}^{\mathrm{miss}})$, the transverse mass of the two leading jets and the missing transverse momentum, which can partially reconstruct the decayed sextet scalar if its decay involves a neutrino but also displays a low peak around the sextet mass when the neutrino is the recoiling particle. We compare our custom search to the most up-to-date existing analyses that exhibit some sensitivity to our signal processes. Some searches are sensitive to the mostly-visible channel, or some flavor-exclusive subchannel, while others probe the "semi-invisible" channel, which has zero charged leptons and is thus characterized only by jets and missing energy. In all cases, we impose LHC bounds in the (m_Φ, Λ) plane of EFT parameters assuming the Run 2 integrated luminosity of $\mathcal{L} = 139$ fb^{-1} (or the true luminosities of the recast analyses), and we offer projections for the HL-LHC dataset.

This paper is organized as follows. Section II is devoted to a discussion of the model, including the LHC production and decays of the sextet scalar. In Sec. III we enumerate the signal processes of interest and detail the signal simulation and analysis procedures. Section IV concerns the semi-invisible (jets + $E_{\mathrm{T}}^{\mathrm{miss}}$) channel, which in principle can constrain both single and pair production of our sextet scalar. Section V is dedicated to our custom search for singly produced sextet scalars in the mostly visible (jets + lepton + $E_{\mathrm{T}}^{\mathrm{miss}}$) channel, with comparisons made to existing searches whose limits are already quite strong. Section VI combines the novel and recast analyses to provide a comprehensive map of current-day limits and projections for the HL-LHC. Section VII concludes.

II. MODEL DISCUSSION

We begin by introducing the effective theory of color-sextet scalars to be analyzed in this work. We consider a minimal model of sextet interactions with Standard Model fermions. If the scalar has weak hypercharge $Y = 1/3$, it can couple both to quark pairs of mixed type (one up, one down) and to color-charged particles accompanied by a lepton. But these interactions cannot be simultaneously realized without inducing lepton number (L) nonconservation. We suppose that L is conserved and that the sextet scalar has lepton number $L = -1$, so that its leading interactions with the Standard Model, apart from gauge interactions, are given by

$$\mathcal{L} \supset \frac{1}{\Lambda^2} J^{sia} \Phi_s G_{\mu\nu a} \times (\lambda_{\mathrm{L}}^{IX} \overline{Q_{\mathrm{L}Ii}^{\mathrm{c}}} \cdot \sigma^{\mu\nu} L_{\mathrm{L}X} + \lambda_{\mathrm{R}}^{IX} \overline{u_{\mathrm{R}Ii}^{\mathrm{c}}} \sigma^{\mu\nu} \ell_{\mathrm{R}X}) + \mathrm{H.c.} \quad (2)$$

with spinor and $\mathrm{SU}(2)_{\mathrm{L}}$ indices implicit.[1] The superscript$^{\mathrm{c}}$ denotes charge conjugation and subscripts$_{\mathrm{R}}$ denote right handedness (chirality). The tensor $\sigma^{\mu\nu} = (\mathrm{i}/2)[\gamma^\mu, \gamma^\nu]$ performs a chirality flip. The couplings $\lambda_{\mathrm{L,R}}$ form matrices in quark and lepton generation space, with I or $X = 3$ labeling the heavy generation(s). Finally, the coefficients J are the generalized Clebsch-Gordan coefficients [3] required to construct gauge-invariant contractions of the direct-product representation $\mathbf{3} \otimes \mathbf{6} \otimes \mathbf{8}$ in SU(3) [7]. These 144 coefficients relate the generators of the $\mathbf{6}$ of SU(3) to the generators of $\mathbf{3} \otimes \mathbf{8}$ according to

$$[t_{\mathbf{6}}^a]_s{}^t = -\{J^{sib} \bar{J}_{tcj} [t_{\mathbf{3}\otimes\mathbf{8}}^a]_{ib}{}^{jc}\}^*, \quad (3)$$

[1]The dot $\cdot$ denotes an antisymmetric contraction of the $\mathrm{SU}(2)_{\mathrm{L}}$ doublets, so that the weak singlet is explicitly written as $\overline{Q_{\mathrm{L}A}^{\mathrm{c}}} \epsilon^{AB} L_{\mathrm{L}B}$ with $A, B \in \{1, 2\}$ and ϵ the two-dimensional totally antisymmetric symbol.

with $\bar{J}_{sai} \equiv [J^{sia}]^\dagger$ denoting Hermitian conjugation, and are normalized according to tr $J^s \bar{J}_t = \delta^s{}_t$. In the basis where the generators t_3 of the fundamental representation of SU(3) are proportional to the Gell-Mann matrices, these Clebsch-Gordan coefficients can be written as

$$J^{sia} = -\mathrm{i}\epsilon^{ijk}[t_3^a]_j{}^l \bar{K}^s{}_{lk}, \tag{4}$$

where ϵ^{ijk} is the totally antisymmetric symbol and $K_s{}^{lk}$ are the lk-symmetric coefficients for the direct product $\mathbf{3} \otimes \mathbf{3} \otimes \bar{\mathbf{6}}$ of SU(3), which appear in models of sextet diquarks mentioned in (1) and are tabulated in a few places [3,5].

A. Scalar pair production at LHC

It is worthwhile to establish some basic results before discussing the LHC phenomenology of our model. Pair production of the sextet scalar is guaranteed by gauge invariance and can have a large cross section at the LHC for sufficiently light sextets. This process is represented by the diagrams shown in Fig. 1. The gg initial states provide the bulk of the production at proton colliders. To be more specific, at the $\sqrt{s} = 13$ TeV LHC, the production rate exceeds 1 pb for $m_\Phi \lesssim 750$ GeV [3,5], thus not much smaller than the rate of color-octet scalar pair production [10]. The leading-order (LO) cross sections for this process are displayed in Fig. 3, in Sec. III, following the requisite details about signal simulation.

B. Single scalar production

While sextet pair production is unavoidable, we are principally interested in the single-production processes available in this specific realization. This interest stems from the competitive cross sections (in some parameter space) and distinct kinematic features of resonant sextet production, which—as we show later—makes single production the superior experimental target, increasingly so for heavier sextets. The parton-level cross section for a given initial up-type quark u_I and final-state charged (anti-)lepton ℓ_X^+ can be expressed in the massless-quark limit as

$$\begin{aligned}\hat{\sigma}(u_I g \to \ell_X^+ \Phi^\dagger)(\hat{s}) = &\frac{1}{64\pi}\left[\left(\frac{\lambda_{\mathrm{L}}^{IX}}{\Lambda^2}\right)^2 + \left(\frac{\lambda_{\mathrm{R}}^{IX}}{\Lambda^2}\right)^2\right] \\ &\times \frac{1}{\hat{s}}(\hat{s} - m_\Phi^2 + m_\ell^2) \\ &\times [m_\ell^4 - 2m_\ell^2(\hat{s} + m_\Phi^2) + (\hat{s} - m_\Phi^2)^2]^{1/2},\end{aligned} \tag{5}$$

which further collapses to

$$\hat{\sigma}(u_I g \to \ell_X^+ \Phi^\dagger)(\hat{s}) \approx \frac{1}{64\pi}\left[\left(\frac{\lambda_{\mathrm{L}}^{IX}}{\Lambda^2}\right)^2 + \left(\frac{\lambda_{\mathrm{R}}^{IX}}{\Lambda^2}\right)^2\right]\frac{1}{\hat{s}}(\hat{s} - m_\Phi^2)^2 \tag{6}$$

in the massless-lepton limit. These results reduce to those introduced in previous work [9] if $\lambda_{\mathrm{L}}^{IX} \to 0$. The novel focus of this work is single production in association with a neutrino ν_X. The parton-level cross section for this process with an initial down-type quark d_I can be written (in the same limits as above) as

$$\begin{aligned}\hat{\sigma}(d_I g \to \nu_X \Phi^\dagger)(\hat{s}) = &\frac{1}{64\pi}\left(V_{I'I}^{\mathrm{CKM}}\frac{\lambda_{\mathrm{L}}^{I'X}}{\Lambda^2}\right)^2 \\ &\times \frac{1}{\hat{s}}(\hat{s} - m_\Phi^2 + m_\nu^2) \\ &\times [m_\nu^4 - 2m_\nu^2(\hat{s} + m_\Phi^2) + (\hat{s} - m_\Phi^2)^2]^{1/2}\end{aligned} \tag{7}$$

and

$$\hat{\sigma}(d_I g \to \nu_X \Phi^\dagger)(\hat{s}) \approx \frac{1}{64\pi}\left(V_{I'I}^{\mathrm{CKM}}\frac{\lambda_{\mathrm{L}}^{I'X}}{\Lambda^2}\right)^2\frac{1}{\hat{s}}(\hat{s} - m_\Phi^2)^2. \tag{8}$$

In these expressions $\hat{s}$ is the partonic center-of-mass energy. In the expressions for neutrinos, V^{CKM} is the CKM matrix [11,12]. Summation is to be understood over the quark generation index I'. Clearly the neutrino cross section (7) is closely related to the charged-lepton result (5).

C. Decays of the sextet scalar

If only the right-handed couplings λ_{R} are nonvanishing, then the sextet scalar decays only to a gluon, a down-type quark, and a charged lepton. In general, with all couplings $\lambda_{\mathrm{L,R}}$ permitted, the partial width to each charged-lepton channel can be expressed as

$$\begin{aligned}\Gamma(\Phi \to \ell_X^+ \bar{u}_I g) = &\frac{1}{(2\pi)^3}\frac{1}{8m_\Phi^3}\left[\left(\frac{\lambda_{\mathrm{L}}^{IX}}{\Lambda^2}\right)^2 + \left(\frac{\lambda_{\mathrm{R}}^{IX}}{\Lambda^2}\right)^2\right] \\ &\times \int_{m_\ell^2}^{(m_\Phi - m_u)^2} \mathrm{d}s_{13}\mathcal{F}(s_{13}, m_\Phi, m_u, m_\ell),\end{aligned} \tag{9}$$

where $s_{13} = (p_1 + p_3)^2$ is the invariant squared mass of the lepton-gluon subsystem (an arbitrary choice), and where

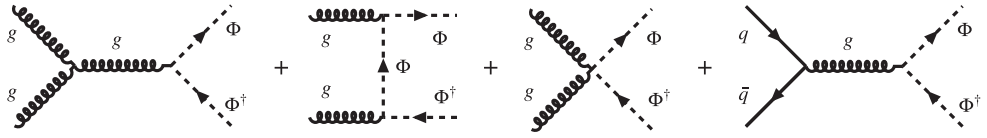

FIG. 1. Parton-level diagrams for Φ pair production at LHC.

$$\mathcal{F}(s_{13}, m_\Phi, m_u, m_\ell) = \frac{1}{s_{13}^2}(s_{13} - m_\ell^2)^3(m_\Phi^2 - m_u^2 - s_{13}) \times [m_u^4 - 2m_u^2(m_\Phi^2 + s_{13}) + (m_\Phi^2 - s_{13})^2]^{1/2} \quad (10)$$

is proportional to the squared transition amplitude integrated over $s_{23} = (p_2 + p_3)^2$. The integral in (9) does not admit an analytical result, except in the massless-fermion limit with $\mathcal{F}(s_{13}) \approx s_{13}(m_\Phi^2 - s_{13})^2$ in which

$$\Gamma(\Phi \to \ell_X^+ \bar{u}_I g) \approx \frac{2}{3}\frac{1}{(8\pi)^3}\left[\left(\frac{\lambda_{\mathrm{L}}^{IX}}{\Lambda^2}\right)^2 + \left(\frac{\lambda_{\mathrm{R}}^{IX}}{\Lambda^2}\right)^2\right] m_\Phi^5, \quad (11)$$

but can be evaluated numerically in the general case. Of course, if any element of λ_{L} is nonvanishing, then Φ can also decay to a gluon, a down-type quark, and a neutrino. The partial widths for these channels, $\Gamma(\Phi \to \nu_X \bar{d}_I g)$, are given by (9) and (11) with the replacements

$$m_u \to m_d, 4m_\ell \to m_\nu \approx 0, \quad \text{and} \quad \left(\frac{\lambda_{\mathrm{L}}^{IX}}{\Lambda^2}\right)^2 + \left(\frac{\lambda_{\mathrm{R}}^{IX}}{\Lambda^2}\right)^2 \to \left(V_{I'I}^{\mathrm{CKM}}\frac{\lambda_{\mathrm{L}}^{I'X}}{\Lambda^2}\right)^2. \quad (12)$$

For $m_\Phi \gg m_u, m_d, m_\ell$, if the couplings λ_{L} are of equal size, the total charged-lepton and neutrino branching ratios are each nearly 50%. We restrict ourselves to parameter space in which the sextet scalar decays promptly, which is the case for all but the lightest sextets with very high ($\mathcal{O}(10)$ TeV) EFT cutoffs.

D. Computer implementation and benchmark scenarios

For analytic and numerical investigation, we implement this model in FEYNRULES version 2.3.43 [13,14], a package for *Mathematica*© version 12.0 [15]. We check our analytic results with the help of FEYNCALC version 9.3.0 [16–18], using as input a FEYNARTS model file generated by FEYNRULES. Event samples are produced using MADGRAPH5_AMC@NLO (MG5_AMC) version 3.3.1 [19,20], the input for which is a Universal FeynRules Output (UFO) also produced by FEYNRULES [21]. Notes on the UFO implementation of the unique color structure in (2), which is not natively supported by this toolchain, are available in [7].

We are presently interested in collider signatures involving hard light-flavor or flavorless jets, significant amounts of missing transverse energy, and in some cases a charged lepton $\ell^\pm$. Representative diagrams for the single-sextet processes of interest are displayed in Fig. 2. For simplicity, we explore scenarios where the color-sextet scalar couples only to first- and second-generation left-chiral fermions, so that for instance $\ell \in \{e, \mu\}$. In some scenarios, to derive the strongest bounds from recast analyses, we allow couplings

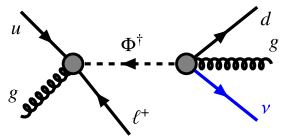

(a) Diagram for production in association with a lepton followed by decay involving a neutrino.

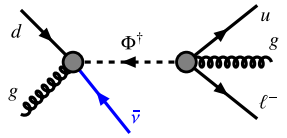

(b) Similar to above for the reverse process with neutrino at the production step.

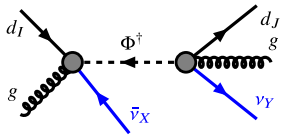

(c) Diagram for the all-neutrino process.

FIG. 2. Diagrams for $\Phi^\dagger$ production at LHC (Φ has $\bar{q}g$ initial states with lower parton luminosity) followed by three-body decay. Blobs denote dimension-six effective vertices.

only to e or μ; we clarify in later sections when this is the case. In summary, we take

$$\lambda_{\mathrm{L}}^{IX} = 1 \ \text{ for } I, \quad X \in \{1,2\} \ \text{ and } \ \lambda_{\mathrm{R}}^{IX} = 0. \quad (13)$$

An investigation of the opposite scenario, with only elements of λ_{R} nonvanishing, is provided in [9]. As mentioned above, any nonvanishing λ_{L} inevitably generates couplings to both charged leptons and neutrinos, hence the total width $\Gamma(\Phi)$ includes decays to charged leptons and the exclusive cross sections of the processes in Fig. 2 are affected accordingly.

Before we move on, it is appropriate to discuss the range of validity of the effective operator (2) and the resulting allowed values of the cutoff Λ. It is widely understood that effective operators can only accurately describe physical processes taking place at energy scales lower than the scale of the degrees of freedom integrated out of some ultraviolet theory in order to produce the infrared model. This physical constraint implies some relationship between the scale Λ, the energy scale of a physical process of interest, and perhaps the mass(es) of the infrared modes. In previous work, we computed the perturbative unitarity bound [22–24] on the right-chiral part of the operator (2) and used a simulation-driven approach to avoid parameter space violating the limit. A similar analysis can be performed for the left-chiral part, which gives a lower bound proportional to

$$\Lambda_{\mathrm{min}}^2 \propto \lambda_{\mathrm{L}}^{IX}(\hat{s} - m_\Phi^2) \quad (14)$$

with $\hat{s}$ the partonic center-of-mass energy of the sextet scalar production process. We use the full result, which can be found by comparison with [9], to define the edge of the valid EFT parameter space in the (m_Φ, Λ) plane for the purpose of limit calculation in Sec. VI.

III. SIGNAL SIMULATION AND STATISTICAL ANALYSIS

In this section we lay the groundwork for the analyses in Secs. IV and V by detailing the simulation of the signal processes and describing the statistical analysis procedures. The intent is to relegate most technical details here in order to leave Secs. IV–VI free to focus on phenomenology.

A. Signal samples

Our multifaceted analysis requires a number of signal samples with a variety of final states in a large parameter space. Most of the important samples are for resonant sextet scalar production. In this category, we simulate

(i) $pp \to \ell^- \Phi$, $\Phi \to \bar{\nu}\, \bar{d}\, g$ ($\ell \in \{e, \mu\}$),
(ii) $pp \to \nu \Phi$, $\Phi \to \ell^+ \bar{u} g$, and
(iii) $pp \to \nu \Phi$, $\Phi \to \bar{\nu}\, \bar{d}\, g$

and their conjugate processes.[2] We categorize the first two processes as "mostly visible" and the latter as "semi-invisible", as a shorthand for the lepton/neutrino content. All processes feature visible hard jets. We prepare both a set of samples inclusive with respect to (light) lepton flavor and separate sets including only $e^\pm$ or $\mu^\pm$, since the latter are required to pass selections for two recast searches discussed in Sec. IV. We reiterate that the couplings $\lambda_{\rm L}^{IX}$ are set to unity only for the needed flavors I, X in each case. Heavy quarks and leptons are not considered in this study. These single-production processes are simulated in MG5_AMC version 3.3.1 at leading order for an LHC center-of-mass energy of $\sqrt{s} = 13$ TeV. The scattering amplitudes are convolved with the NNPDF 2.3 LO set of parton distribution functions [25] with renormalization and factorization scales $\mu_{\rm R}, \mu_{\rm F}$ fixed equal to m_Φ. Showering and hadronization is performed by PYTHIA8 version 8.244 [26]. For computation of the yields, the signals are normalized to the cross sections reported by MG5_AMC after appropriate color-factor correction [9]. As demonstrated in Sec. II, the normalizations are proportional to Λ^{-4}; rescaling is done wherever required in order to explore the Λ dimension of the (m_Φ, Λ) EFT parameter space. Some example cross sections for production in association with a single lepton or neutrino flavor are displayed in Fig. 3. These single-production cross sections are computed assuming first-generation SM fermions only and an EFT cutoff $\Lambda = 3$ TeV. This choice of cutoff renders these results self-consistent within the EFT framework, following the discussion in Sec. II. In this scenario, the cross sections are of $\mathcal{O}(10\text{–}100)$ fb at the TeV scale.

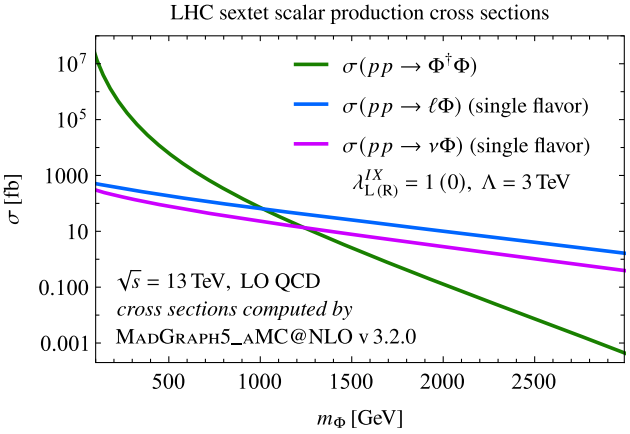

FIG. 3. Leading-order inclusive LHC cross sections of color-sextet scalar pair and single production at center-of-mass energy $\sqrt{s} = 13$ TeV. Single production is considered for one ℓ/ν flavor in benchmark scenario with EFT cutoff $\Lambda = 3$ TeV.

Figure 3 also depicts the leading-order cross sections of sextet scalar pair production, which we mentioned in Sec. II and include in our analysis in the interest of completeness. We simulate pair production followed by both mostly visible and semi-invisible decays in view of the analyses to be reinterpreted in our model framework (*viz.* Secs. IV and V). The events are generated at LO in MG5_AMC and showered with PYTHIA8, and the signal normalizations are computed with renormalization and factorization scales set again to $\mu_{\rm R} = \mu_{\rm F} = m_\Phi$. Note that pair production, which proceeds through gauge interactions, has an inclusive rate independent of the EFT parameters in (2). The exclusive cross sections depend on $\lambda_{\rm L}^{IX}\Lambda^{-2}$, but as noted in Sec. II our simple benchmark values imply branching fractions $\beta(\Phi \to \ell^+ \bar{u} g) \approx \beta(\Phi \to \bar{\nu}\, \bar{u}\, g) \approx 1/2$ for a given generation.

B. Limit setting and significance calculation

On a technical level, this study contains two kinds of analysis. There are three cases in which we identify an existing search executed by one of the LHC collaborations that may be sensitive to our color-sextet scalar signals containing, at minimum, jets and $E_{\rm T}^{\rm miss}$. We reinterpret the null results of these searches within our model framework in order to impose limits on m_Φ, and Λ where appropriate, which are valid today—based on the integrated luminosity used for each analysis—and then projected into the future *via* luminosity rescaling. These reinterpretations are performed using MADANALYSIS5 (MA5) version 1.9.20 [27], which in its reconstruction mode ($-$R) can run any of the validated recasted LHC analyses available on the MA5 Public Analysis Database (PAD) [28–30].

When called in reconstruction mode, MA5 accepts as input a HEPMC event record produced by PYTHIA8. Once

[2]Recall that the unusual presence of two anti-fermions in the final states arises from the color conjugation of the quark in (2).

one or more analyses on the PAD are chosen for execution by the user, MA5 simulates the ATLAS or CMS detector (whichever is needed for the analysis at hand) either by calling DELPHES3 version 3.4.3 [31,32] or, for more recent recasts, by using its inbuilt Simplified Fast Detector Simulation (SFS) module [33]. In either case, the simulated detector response is parametrized by an analysis-specific card tuned during the development of the recast in order to optimize the agreement between recast and official results. Meanwhile, object reconstruction is performed by FASTJET version 3.4.0 [34]. The reconstructed event sample is then analyzed by the `SampleAnalyzer` core of MA5, which imposes the analysis selection criteria and records the sample efficiency under each cut. With this done, MA5 finally computes the upper limit(s) at 95% confidence level (CL) [35] on an arbitrary new-physics cross section with the efficiency of the provided sample. When an analysis comprises multiple signal regions, a limit is computed for each. MA5 computes the expected limit, based on the expected background yields provided by the experimental collaboration, and the observed limit based on the true event yield. If the user supplies a signal cross section at the import step, MA5 further computes the significance $1-\mathrm{CL}_s$ of the sample, which is ruled out at 95% CL if $1-\mathrm{CL}_s \geq 0.95$. Our final note is on luminosity rescaling for extrapolation to HL-LHC: MA5 provides a number of options to estimate the expected limits at 95% CL from a present-day analysis hypothetically re-run in the future on a larger dataset. Any new integrated luminosity can be chosen by the user for extrapolation. The signal and (central) background yields are rescaled linearly with the luminosity. The user can choose how the background uncertainties are rescaled; we use the default option, whereby the systematic uncertainties are rescaled linearly, the statistical uncertainties are rescaled by the square root of the luminosity, and these components are added in quadrature [36].

The reinterpretation of existing analyses very helpfully paints a picture of the real-life experimental status of our theory. As alluded to in multiple places, however, the crux of this work is a dedicated search we tailor to the unique features of our leptonic sextet processes. We use a different workflow and our own statistical tools to evaluate the sensitivity of our custom analysis. In particular, we use the MADANALYSIS5 SFS module to perform detector simulation and object reconstruction for all of our signal and background samples. We use an SFS card optimized for the ATLAS detector. We then feed the (relevant) reconstructed event files to MA5 once again, this time imposing our own selection criteria and recording the efficiencies as usual.

At this stage, our workflow diverges from what is outlined above for reinterpretation because we carry out a joint-likelihood analysis and use measures of the significance for exclusion and discovery that are not natively available in MADANALYSIS5. To be specific, we compute the significance Z of a signal s (whose uncertainty we neglect) with strength modifier μ, given an expected background $\langle b \rangle$ with non-negligible uncertainty σ_b, according to the asymptotic (large-m) formula $Z_\mu^m = (q_\mu^m)^{1/2}$ [37], where [38]

$$q_\mu^m = -2\ln\frac{\mathcal{L}(m|\mu,\hat{\hat{b}})}{\mathcal{L}(m|\hat{\mu},\hat{b})}, \quad \hat{\mu} \leq \mu, \tag{15}$$

is a frequentist test statistic for one-sided limits based on the ratio of profile likelihoods [39]

$$\mathcal{L}(m|\mu,b) = \prod_{i=1}^{N_{\mathrm{bin}}} \frac{(\mu s_i + b_i)^{m_i}}{m_i!} \mathrm{e}^{-(\mu s_i + b_i)} \times \frac{1}{\sqrt{2\pi}\sigma_{b,i}} \exp\left\{-\frac{1}{2}\frac{(b_i - \langle b_i \rangle)^2}{\sigma_{b,i}^2}\right\}. \tag{16}$$

This expression gives the joint likelihood for N_{bin} bins, which is relevant for our custom analysis with cuts binned in an observable that displays peaks at m_Φ for our signal samples. In this construction, the total event count m_i in each bin i of some observable is assumed to follow a Poisson distribution, while each background b_i is taken as a nuisance parameter constrained (in principle) by a Gaussian-distributed measurement in some control region [40].[3] The bin yields are assumed to be uncorrelated. The quantity $\hat{\hat{b}} = \hat{\hat{b}}(\mu)$ in (15) is the conditional maximum-likelihood (ML) estimator of the background b for a given μ, while the pair $(\hat{\mu},\hat{b})$ are unconditional ML estimators of the likelihood $\mathcal{L}$. It is also possible to define the likelihood for an individual bin by rewriting (16) as

$$\mathcal{L}(m|\mu,b) = \prod_{i=1}^{N_{\mathrm{bin}}} \mathcal{L}(m_i|\mu,b_i). \tag{17}$$

Within this framework, we compute the median significance for exclusion and discovery of our signal using the Asimov datasets according to

$$Z_{\mathrm{excl}} \equiv Z_{\mu=1}^{m=\langle b \rangle} \quad \text{and} \quad Z_{\mathrm{disc}} \equiv Z_{\mu=0}^{m=s+\langle b \rangle}, \tag{18}$$

taking $Z_{\mathrm{excl}} = 1.68$ and $Z_{\mathrm{disc}} = 5$ as our exclusion and discovery thresholds.[4] In this calculation, the background uncertainties σ_b follow from the theoretical cross section uncertainties $\delta\sigma_{\mathrm{theo}}$, which are listed in Sec. V. We compute the test statistic q_μ^m using both the joint likelihood (16) and the individual likelihoods for each bin in (17).

[3]The backgrounds could equally well be taken to be Poisson distributed. The asymptotic Poisson and Gaussian profile likelihood ratios converge in the limit $\sigma_b \to 0$.

[4]In the limit $s/b \ll 1$, which does not apply to all of our parameter space after selections, Z_{disc} reduces to the well known $Z_{\mathrm{disc}} = s/\sqrt{b}$.

The significance(s) (18) derived in the first case give the most optimistic estimates of collider sensitivity to our bSM signal, whereas the significance(s) from the most sensitive individual bin give the most conservative projections. We provide both results in Secs. V and VI in order to give an idea of the *range* of limits one can expect from our dedicated analysis.

IV. A "SEMI-INVISIBLE" SEXTET: JETS + $E_{\mathrm{T}}^{\mathrm{miss}}$

The first channel we consider excludes charged leptons and thus includes only hard jets and missing transverse energy. This search channel can be sensitive to signal processes of the type displayed in Fig. 2(c), which we have been referring to as semi-invisible. Since the jets + $E_{\mathrm{T}}^{\mathrm{miss}}$ signal provides a classic search channel for many popular bSM constructions, including dark matter models and supersymmetric models, there exist limits based on the full Run 2 dataset. We therefore begin by exploring the extent to which existing searches constrain our model. In particular, the MADANALYSIS5 PAD includes a Run 2 search performed by the ATLAS Collaboration for new phenomena in final states with jets and significant missing transverse energy [41]. This analysis was announced as ATLAS-CONF-2019-040 and subsequently relabeled ATLAS-SUSY-2018-22. The data correspond to an integrated luminosity of $\mathcal{L} = 139\ \mathrm{fb}^{-1}$. ATLAS interpreted the null results of this search, ATLAS-CONF-2019-040, for typical scenarios involving squark and gluino pair production; we reinterpret the analysis within our model framework following the workflow described in Sec. III.

This ATLAS analysis requires at least two jets, the harder of which must have at least $p_{\mathrm{T}}(j_1) > 200$ GeV, and at least $E_{\mathrm{T}}^{\mathrm{miss}} > 300$ GeV, with adequate separation between the two or three hardest jets and the missing transverse momentum. The analysis (which consists of a multi-bin subanalysis and a boosted decision tree subanalysis, only the first of which is recast) imposes more stringent requirements on jet multiplicity in some bins. There are furthermore selections on the $E_{\mathrm{T}}^{\mathrm{miss}}$ significance and the effective mass m_{eff}, defined as the scalar sum of $E_{\mathrm{T}}^{\mathrm{miss}}$ and all jets with $p_{\mathrm{T}}(j) > 50$ GeV. These selections powerfully suppress the Standard Model backgrounds, some of which are very large, most notably Z boson production with hard jets followed by the invisible decay $Z \to \nu\bar{\nu}$. Since some bins in the multibin analysis allow more than three hard jets, the search is sensitive to both single and pair production of our color-sextet scalar. We therefore apply this recast analysis to the semi-invisible single-production samples and the pair samples simulated with both sextets decaying to neutrinos. The results are displayed in Fig. 4.

Figure 4(a) shows the upper observed and expected limits at 95% CL on the single-production cross section for a range of sextet masses at the TeV scale. These limits are compared to the cross section in a benchmark scenario with

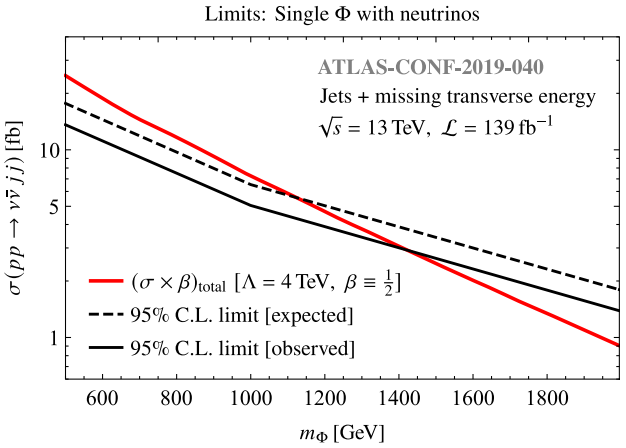

(a) Limits on semi-invisible single sextet production. In a scenario with EFT cutoff $\Lambda = 4$ TeV, the observed (expected) lower bound on m_Φ is 1424 (1124) GeV.

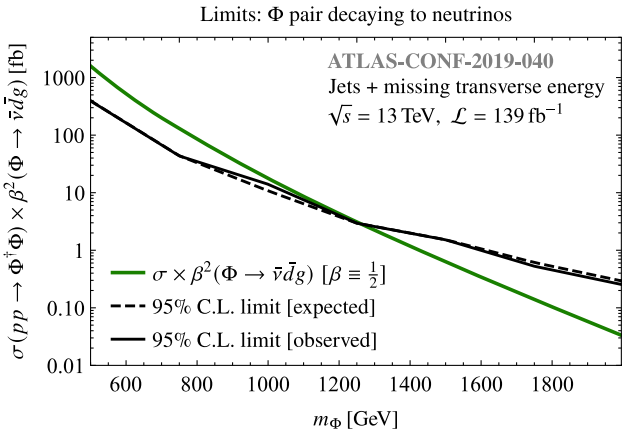

(b) Limits on semi-invisible sextet pair production. Observed and expected lower bounds on m_Φ from this search are nearly coincident at 1262 GeV.

FIG. 4. Observed and expected limits at 95% CL from ATLAS-CONF-2019-040, a Run 2 search for squarks and gluinos in final states with jets and missing transverse momentum.

sextet couplings to first- and second-generation SM fermions and an EFT cutoff of $\Lambda = 4$ TeV. As discussed in Sec. II, and for direct comparison to the analyses in Sec. V, the branching fraction of sextets to neutrino modes is set to $\beta = 1/2$. In this benchmark we obtain an observed lower limit on the sextet mass of $m_\Phi \approx 1424$ GeV, marginally stronger than the expected limit of 1124 GeV due to underfluctuations in the data. Figure 4(b), meanwhile, shows the limits on pair production. The observed limit at 95% CL, which is very close to the expected limit, is at $m_\Phi \approx 1262$ GeV. It is important to note that the pair-production limits, while sensitive to the branching fraction (s) of the scalar to neutrino modes, are independent of the EFT cutoff Λ—provided that it is low enough for the resonance to decay promptly—because the production is

due to gauge interactions. We find it interesting that for pair production, which can be directly compared to the supersymmetric scenario considered by ATLAS, the efficiencies of the sextet samples are not too dissimilar to those of gluino pair production followed by the effective three-body decay $\tilde{g} \to qq'\tilde{\chi}_1^0$ *via* a heavy off-shell squark. The limits are of course not coincident because its pair-production rate is lower than that of the color-octet gluino due to color and spin.

While the limits from the semi-invisible channel are nontrivial, comfortably disfavoring sextet scalars lighter than ∼1 TeV, they turn out to be the weakest bounds calculated in this work. We furthermore find that a custom cut-and-count analysis in this channel cannot significantly improve upon existing Run 2 limits on single sextet production, such that extending the constraints in the channel requires a larger dataset. We briefly demonstrate this difficulty using the selections listed in Table I, which are aimed—but unsuccessful—at exceeding the sensitivity of ATLAS-CONF-2019-040 with a nonequivalent set of cuts. We furthermore show in Fig. 5 some signal and background distributions of observables one might naturally target while crafting a dedicated jets + $E_{\mathrm{T}}^{\mathrm{miss}}$ search. By far the most difficult background to suppress is the aforementioned invisibly decaying Z boson produced with hard jets, which has a cross section of $\mathcal{O}(10^4)$ pb. Figure 5(a) suggests that a quite extreme $E_{\mathrm{T}}^{\mathrm{miss}}$ requirement is a good place to start. But while the semi-invisible signal does have endpoints in certain distributions (for instance, one can see in Fig. 5(b) that the invariant mass $m_{j_1 j_2}$ of the two leading jets has a cusp at m_Φ), we find no observables with a sharp peak. Figure 5(c), for instance, shows that the missing energy significance

$$\mathcal{S}(E_{\mathrm{T}}^{\mathrm{miss}}) = \frac{E_{\mathrm{T}}^{\mathrm{miss}}}{\sqrt{H_{\mathrm{T}}}} \quad \text{with} \quad H_{\mathrm{T}} = \sum_{i=1}^{N_{\mathrm{jet}}} p_{\mathrm{T}}(j_i) \tag{19}$$

is actually *more* sharply peaked for Z + jets than for a $m_\Phi = 2$ TeV signal, though the signal distribution has a

TABLE I. Selection criteria of attempted search for color-sextet scalar produced in association with a neutrino and decaying to $dg\nu$.

Selection criterion	Selection ranges
Jets, anti-k_t $R = 0.4$	$N_{\mathrm{jet}} \geq 2$ $p_{\mathrm{T}}(j) > 100$ GeV, $\lvert\eta(j)\rvert < 2.5$
Charged leptons	VETO e, μ with $p_{\mathrm{T}} > 15$ GeV
b-tagged jets	VETO b-jets with $p_{\mathrm{T}} > 15$ GeV
Leading jet momenta	$p_{\mathrm{T}}(j_1) > 250$ GeV $p_{\mathrm{T}}(j_2) > 250$ GeV
Missing energy, $E_{\mathrm{T}}^{\mathrm{miss}}$	Require $E_{\mathrm{T}}^{\mathrm{miss}} > 750$ GeV

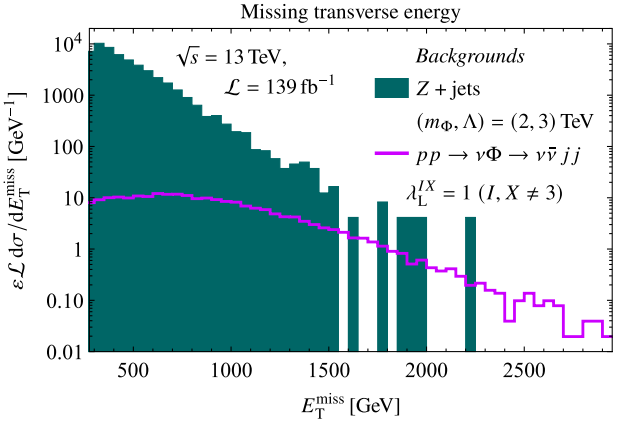

(a) Missing transverse energy in signal and background events surviving all selections in Table I preceding the cut on $E_{\mathrm{T}}^{\mathrm{miss}}$. Distributions are normalized to total yields.

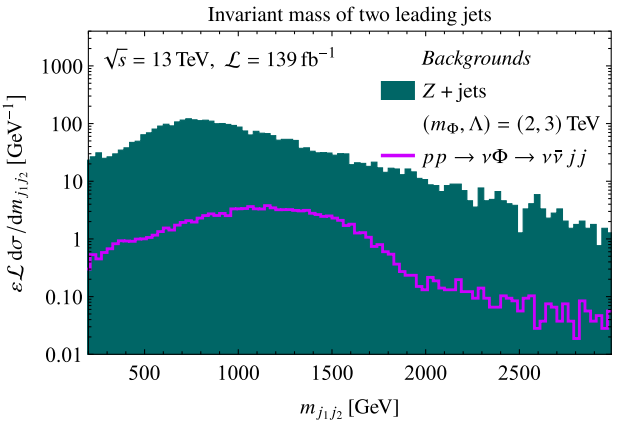

(b) Invariant mass of the leading jet pair in signal and background events surviving all selections in Table I. Distributions are normalized to total yields.

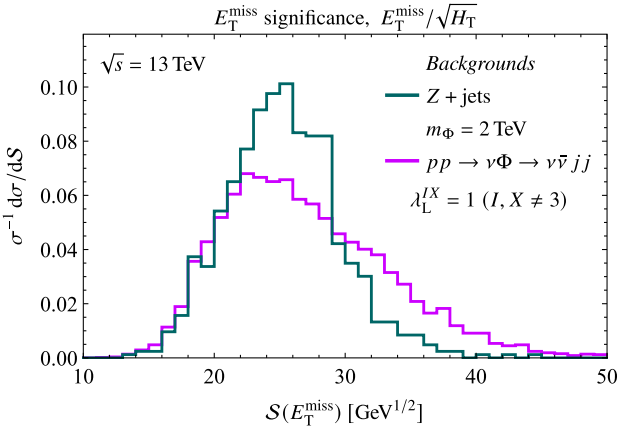

(c) $E_{\mathrm{T}}^{\mathrm{miss}}$ significance in signal and background events surviving all selections in Table I. Distributions are normalized to unity.

FIG. 5. Distributions of three presumably relevant observables in attempted search for color-sextet scalar in the semi-invisible channel. Signal yields are computed for $m_\Phi = 2$ TeV, $\Lambda = 3$ TeV, and $\lambda_{\mathrm{L}}^{IX} = 1$ for $I, X \neq 3$.

slightly fatter tail. The culprit is the unusual contribution to the missing transverse momentum from both the recoiling neutrino and the invisible decay product of the sextet; see once more Fig. 2(c). We therefore find no well motivated selection to impose in addition to, or instead of, the quite stringent requirements of ATLAS-CONF-2019-040. As a result, the limits from the search defined in Table I fail to improve upon the existing bounds: at $\mathcal{L} = 139$ fb^{-1}, for $m_\Phi = 1$ TeV, we can rule out a maximum EFT cutoff of $\Lambda \approx 4$ TeV, and for $m_\Phi = 2$ TeV we are sensitive to no more than $\Lambda \approx 3$ TeV. These limits are quite close to the expected limits from ATLAS-CONF-2019-040 (*viz.* Sec. VI), but no better. At any rate, as we just noted and will demonstrate in the next section, the limits from the semi-invisible channel are far superseded by existing and custom searches in the mostly visible channel, so we set aside the all-neutrino processes until Sec. VI.

V. A "MOSTLY VISIBLE" SEXTET: JETS + ℓ + $E_{\rm T}^{\rm miss}$

The next channel we consider is characterized by hard jets and a single lepton (electron or muon) accompanied by a sizeable amount of missing transverse energy. This channel is populated by signal events of the type displayed in Figs. 2(a) and 2(b), but also by signals in popular bSM scenarios involving dark matter and pair-produced leptoquarks. In this section, we first design a custom search for color-sextet scalars singly produced in this mode. We identify the Standard Model processes with significant overlap for the mostly visible final state and detail their simulation, define selection criteria to exploit the kinematic distinctiveness of our signals, explore a few signal and background distributions, and compare their yields after the common selection. We then recast two existing analyses sensitive to our mostly visible sextet in preparation for a comparison of all bounds in Sec. VI.

A. Single-lepton background processes

There are many Standard Model processes that may be expected to populate this search channel, some with quite large cross sections. The background processes we consider in our analysis are listed in Table II. This table lists the most accurate available cross sections at a center-of-mass energy of $\sqrt{s} = 13$ TeV, along with estimates of the theoretical uncertainties, given in most cases by adding the scale and parton distribution function (PDF) uncertainties in quadrature. These cross sections are exclusive whenever a decay is specified in the table. The largest backgrounds *a priori* are leptonically decaying W boson production in association with hard jets, $t\bar{t}$ production, and single-top production with a light quark (qt). Weak boson pair production leading to final states with exactly one lepton is a potentially important background that survives the b-jet veto that decimates the top quark processes. On the other hand, diboson events with jets and missing energy can be discarded. The same applies to Z + jets since we simultaneously demand exactly one lepton and large $E_{\rm T}^{\rm miss}$. For completeness, we provide some simulation details for each sample used in our analysis.

We simulate the W + jets process in MG5_AMC version 3.3.1 at LO with up to two additional partons included in the hard-scattering matrix element. The scattering amplitude is convolved with the NNPDF 2.3 LO set of parton distribution functions [25] with renormalization and factorization scales $\mu_{\rm R}, \mu_{\rm F}$ fixed equal to m_W. The LO hard-scattering events are matched to parton showers in the MLM scheme [52] at a scale of 30 GeV with the aid of PYTHIA8 version 8.244 [26]. The signal is normalized to the

TABLE II. Leading background processes generating final states with two hard jets, one (charged) lepton, and considerable missing transverse energy. Single W and t denote aggregate particle + antiparticle processes while q denotes light quarks. LHC cross sections for $\sqrt{s} = 13$ TeV are displayed at indicated precision along with total theoretical uncertainties and event descriptions where helpful. Cross sections are inclusive unless decay is specified.

Background process	$\sigma_{\rm LHC}^{13\ \rm TeV}$ (pb)	$\delta\sigma_{\rm theo}$ (%)	Notes
W + jets, $W \to \ell\nu$	20 400.0	1.30	NNLO QCD + NLO EW [42–44] Up to 2 additional partons in ME
Diboson ($WW/WZ/ZZ$)	55.73	6.00	NLO QCD [45,46] Final state includes one lepton
$t\bar{t}$	833.9	4.37	NNLO QCD + NNLL [47]
$t\bar{t} + Z$	0.7587	29.8	NLO QCD from MG5_AMC
$t\bar{t} + W$	0.5662	29.8	NLO QCD [19,48] Up to 2 additional partons in ME
t-channel single top (qt)	214.2	1.49	NNLO QCD [49,50]
tW	79.3	3.30	NLO QCD + NNLL [51]
tZ ($qt + \nu\bar{\nu}$ including nonresonant Z)	0.1399	3.30	NLO QCD from MG5_AMC

cross section at next-to-next-to-leading-order (NNLO) in the strong coupling with next-to-leading order (NLO) electroweak corrections, as computed by FEWZ version 3.1 [43,44] with the NNPDF 3.0 NNLO parton distribution functions [53]. Pair production of weak bosons decaying to one lepton, which includes the processes $WW \to \ell\nu jj$ and $WZ \to \ell\nu jj$, is simulated at LO in MG5_AMC, including interference from virtual photons γ^*. For efficiency optimization, these are divided into single-lepton and zero-lepton samples. The signal normalizations are computed at NLO in the strong coupling using POWHEG-BOX version 2 with the CT10 NLO PDF set [54–57]. The renormalization and factorization scales are set dynamically to $\mu_R = \mu_F = m_{V_1V_2}/2$.

Top pair production is simulated at LO in MG5_AMC. We use a top quark mass of $m_t = 172.5$ GeV for all relevant processes. We again use the NNPDF 2.3 LO parton distribution functions but this time set $\mu_R = \mu_F = m_t$. The normalization of this sample is computed by TOP++ 2.0 for our choice of m_t at NNLO, including resummation of next-to-next-to-leading logarithmic (NNLL) soft-gluon terms [47], with the NNPDF 3.0 NNLO PDF set. Production of $t\bar{t}$ in association with a weak boson is simulated at LO in MG5_AMC along similar lines as previous samples. The $t\bar{t} + Z$ cross section is computed at NLO in QCD in MG5_AMC using the NNPDF 3.0 NLO PDF set, with $\mu_R = \mu_F = m_t$; whereas the $t\bar{t} + W$ cross sections are computed at NLO in QCD using the parton-level integrator MCFM [58] with the MSTW2008 NLO PDF set. We note that the best uncertainty estimates we can find [48] indicate larger uncertainties for the $t\bar{t} + V$ processes than for the other backgrounds in this analysis.

Production of a single top quark in association with a light quark is simulated at LO in MG5_AMC within the five-flavor scheme (bottom quark mass set to $m_b = 0$), since the parton-level process is $qb \to q't$. The sample is normalized to the cross section computed at NNLO in QCD [49] with $\mu_R = \mu_F = m_t$ and with the five-flavor CT14 NNLO PDF set [59]. tW production is similarly simulated in the five-flavor scheme, since the parton-level process is $gb \to tW^-$; our sample is produced at LO and the normalization is computed at NLO in QCD with NNLL resummation [51] with the five-flavor NNPDF 3.1 NLO PDF set [60]. Finally, the relatively small tZ process is simulated at LO in QCD in MG5_AMC, and the cross section is computed at NLO in QCD using the same setup with $\mu_R = \mu_F = m_t$ and using the NNPDF 3.0 NLO PDF set.

B. Selection criteria; distributions and yields

The common selections for our dedicated analysis are listed in Table III. The two leading jets from our signal events are expected to have roughly equal transverse momentum and should be much harder than the leading jets from Standard Model backgrounds. Our baseline selection therefore requires at least two jets with anti-k_t radius parameter $R = 0.4$ to have transverse momentum greater than 100 GeV and pseudorapidity $|\eta| < 2.5$. We then require the leading and second-leading jets to have p_T greater than 250 GeV and 200 GeV, respectively. Many of the processes in Table II involving W bosons also involve top quarks; since our sextet scalar does not couple to third-generation SM fermions, we impose a veto on b-tagged jets. The combination of the b-jet veto and jet p_T requirements (especially the cut on the second-leading jet momentum) so powerfully suppresses the events including top quarks that, at this stage of the analysis, the background is dominated by $W +$ jets, with single-lepton diboson events still surviving but subleading. From here, the selection is therefore dedicated almost entirely to suppressing the leptonically decaying W events.

TABLE III. Common selection criteria of proposed search for color-sextet scalar produced in association with a lepton (neutrino) and decaying to $dg\nu$ ($ug\ell$).

Selection criterion	Selection ranges
Jets, anti-k_t $R = 0.4$	$N_{\text{jet}} \geq 2$ $p_T(j) > 100$ GeV, $\lvert\eta(j)\rvert < 2.5$
Charged leptons	$N_\ell = 1$ $p_T(\ell) > 15$ GeV
b-tagged jets	VETO b-jets with $p_T > 15$ GeV
Leading jet momenta	$p_T(j_1) > 250$ GeV $p_T(j_2) > 200$ GeV
Lepton momentum	$p_T(\ell) > 250$ GeV
Missing energy, E_T^{miss}	Require $E_T^{\text{miss}} > 300$ GeV
Jet-E_T^{miss} separation	$\Delta\phi(j_1, \vec{p}_T^{\text{miss}}) \notin [2\pi/3, 4\pi/3]$

The single lepton in the signal events should be similarly hard and provide a good discriminant from the $W +$ jets background (though it will not by itself sufficiently suppress this process). The lepton p_T distributions are displayed in Fig. 6 for the backgrounds surviving all cuts preceding that on $p_T(\ell)$ (of which only $W +$ jets is visible on this scale), as well as for the pair of signal events corresponding to Figs. 2(a) and 2(b) for a sextet mass of $m_\Phi = 2$ TeV and an EFT cutoff of $\Lambda = 4$ TeV. This figure shows a clear difference not only betwen signals and backgrounds but also between the two types of signal event. In particular, we find that the lepton is much harder when it recoils off of the sextet at the production stage than when it is a decay product of the scalar resonance. We find that a requirement of $p_T(\ell) > 250$ GeV already suppresses over 90% of the remaining $W +$ jets events while accepting most signal events, especially for heavy sextets.

The lepton p_T cut, followed by a requirement of more than 300 GeV of missing transverse energy, effectively eliminate the already decimated top quark backgrounds. The E_T^{miss} cut also culls some remaining $W +$ jets and diboson events, but

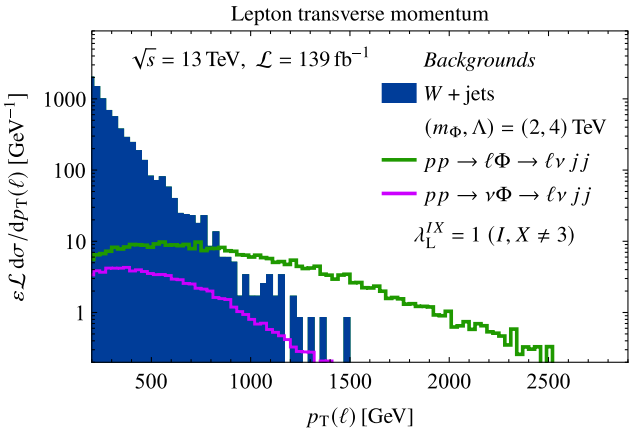

FIG. 6. Transverse momentum of the lepton in signal ($m_\Phi = 2$ TeV) and background events surviving all selections in Table III preceding the cut on $p_T(\ell)$. Distributions are normalized to total yields at $\mathcal{L} = 139$ fb^{-1}.

at this stage the analysis is still fairly weak because of the sheer size of the first background. The final common selection takes another important step toward suppressing this background by forbidding the leading jet from being antiparallel to the missing transverse momentum. Figure 7 shows that the backgrounds surviving all cuts up to and including the lepton p_T requirement have distributions of azimuthal $j_1 - \vec{p}_T^{\,\text{miss}}$ separation, $\Delta\phi(j_1, \vec{p}_T^{\,\text{miss}})$, peaked around π, whereas the signals—particularly the lepton-first events corresponding to Fig. 2(a)—are much flatter in this observable. We therefore find that requiring $\Delta\phi(j_1, \vec{p}_T^{\,\text{miss}}) < 2\pi/3$, or $> 4\pi/3$, is quite effective.

Finally we consider the possibility of strengthening the analysis by finding an observable on which to make binned cuts. One simple approach is to identify an observable that is sharply peaked on at least one side of the sextet scalar mass, such that a set of nonoverlapping bins can be established and a joint likelihood can be computed according to the procedure in Sec. III. Our situation is interesting in that each of the processes represented by Figs. 2(a) and 2(b) has its own well suited observable that does not apply particularly well to the other. In particular, if the lepton is a decay product of the sextet, then the sextet is fully reconstructible using the invariant mass $m_{j_1 j_2 \ell}$ of the leading jets and lepton. As shown in Fig. 3, however, this neutrino-first process suffers from lower cross sections than its lepton-first counterpart, whose $m_{j_1 j_2 \ell}$ distribution is not peaked at m_Φ. It turns out to be better to preferentially target the larger lepton-first process in Fig. 2(a), in which the sextet scalar is partially reconstructible with the transverse mass $m_T(j_1 j_2, E_T^{\text{miss}})$ of the system composed of the two leading jets and the missing transverse momentum. Here and below, we use

$$m_T(A,B) = \sqrt{2p_T(A)p_T(B)[1-\cos\Delta\phi(\vec{p}_T(A),\vec{p}_T(B))]} \tag{20}$$

to denote the transverse mass of a pair $\{A, B\}$, keeping in mind that A or B could itself be a system (such as in the current discussion, where $A = j_1 j_2$). Here, in analogy with the previous paragraph, $\Delta\phi$ is the azimuthal separation between transverse momentum vectors. We show in Fig. 8 the distributions of $m_T(j_1 j_2, E_T^{\text{miss}})$ for the signal and background processes surviving all common selections. This figure shows not only the discrepancy in the yields of the two signal processes but also the clear shelf at m_Φ in the transverse mass distribution of the lepton-first signal. In the interest of simplicity, our final selection requires $m_T(j_1 j_2, E_T^{\text{miss}}) > 250$ GeV and then cuts the transverse mass in 250 GeV-wide bins, terminating at $m_T = 5.0$ TeV. This bin width is particularly well suited to relatively light sextets, whose m_T peaks are quite narrow but which suffer the bulk of the remaining W + jets background. We show

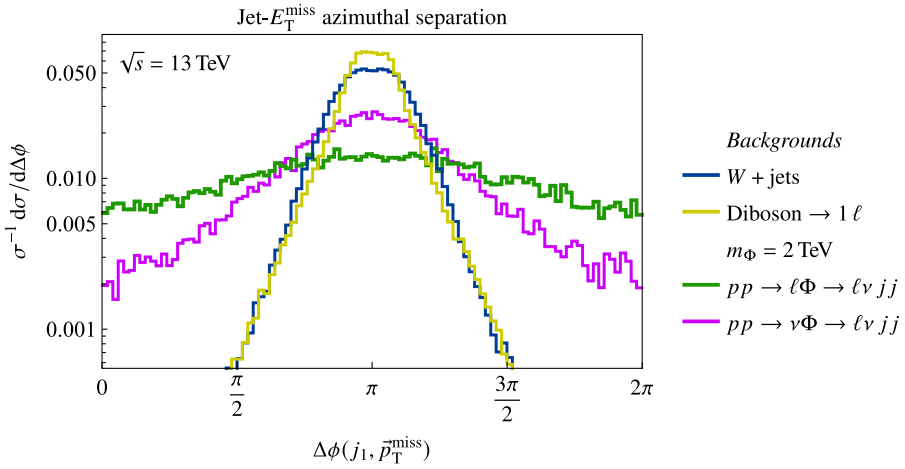

FIG. 7. Azimuthal separation between leading jet and missing transverse momentum in signal ($m_\Phi = 2$ TeV) and background events surviving the selections in Table III up to $p_T(\ell) > 250$ GeV. Distributions are normalized to unity.

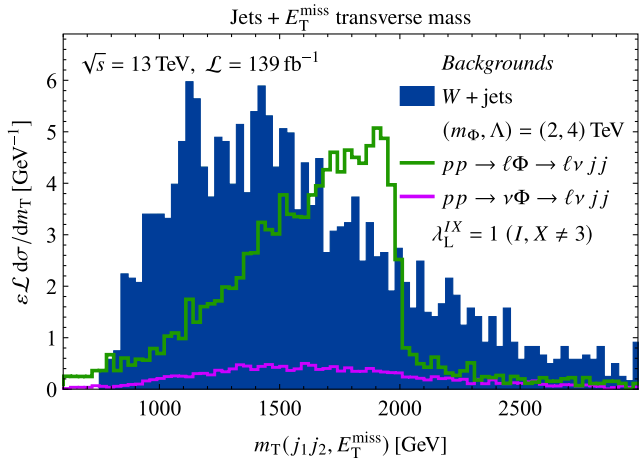

FIG. 8. Transverse mass of the hard-jet system $j_1 j_2$ and missing transverse momentum in signal ($m_\Phi = 2$ TeV) and background events surviving all common selections in Table III. Distributions are normalized to total yields at $\mathcal{L} = 139$ fb^{-1}.

in Table IV the background and signal yields in each bin of the m_T selection (this time for an integrated luminosity of $\mathcal{L} = 3$ ab^{-1}, for some variety). The bulk of the $m_\Phi = 2$ TeV lepton-first events indeed populate the bins just below $m_T = 2.0$ TeV, though there is also a gentle peak below this threshold for neutrino-first events. As discussed in Sec. III, we use the yields for all signals in all bins to compute the signal significance both for the single most sensitive bin and considering the full m_T distribution, assuming no correlations in the interest of extreme simplicity. The results are discussed in Sec. VI.

C. Existing single-lepton analyses

With our dedicated analysis now established, we turn (in the interest of completeness) to two analyses capable of constraining our model using parts of the LHC Run 2 dataset. The first of these is a search by the CMS Collaboration for pair production of scalar leptoquarks coupling exclusively to first-generation Standard Model fermions [61]. This search was announced as CMS-EXO-17-009 and superseded by CERN-EP-2018-265. The relevant part of this analysis is the "$e\nu jj$" channel, in which one leptoquark decays (promptly) to a quark and an electron with branching fraction β and the other leptoquark decays to a quark and a neutrino with branching fraction $1 - \beta$. The luminosity for this analysis is relatively low, $\mathcal{L} = 35.9$ fb^{-1}, but a follow-up analysis including a neutrino channel has not been released.[5]

The $e\nu jj$ selection requires exactly one electron, at least two jets, and $E_T^{miss} > 100$ GeV. Since this analysis targets first-generation leptoquarks, a muon veto is applied. Since signal events are assumed to result from production of two degenerate particles, the transverse masses $\{m_T(j_a, E_T^{miss}), m_T(j_b, e)\}$ are computed with $\{j_a, j_b\}$ chosen from the two hardest jets $\{j_1, j_2\}$ such that the difference in transverse masses is minimized. A number of thresholds are declared for the jet-electron transverse mass, constituting a set of inclusive (overlapping) bins. There is finally an inclusive binned selection on S_T, the scalar sum of transverse momenta of the electron, the two leading jets, and the missing transverse momentum. Much like the ATLAS search in the semi-invisible channel discussed in Sec. IV, there is nothing in this search *a priori* that favors single or pair production of our sextet, since both modes can produce a single electron and a single neutrino. Sextet pair production is expected to produce more than two hard jets from the two three-body decays, but the jet multiplicity requirement in CMS-EXO-17-009 is bounded only from below. We therefore apply the recast of this search, available in the MA5 PAD, to our mostly visible single-production samples (exclusive to electrons) and a set of pair-production samples with one sextet decaying to an electron and the other to a neutrino. The results for single production are displayed in Fig. 9.

In analogy with Sec. IV, this figure shows the upper observed and expected limits at 95% CL on the single-production cross section compared to the theoretical rate in a benchmark with EFT cutoff $\Lambda = 4$ TeV. Here the electron and neutrino branching fractions are both set to $\beta = 1/2$. In this benchmark we obtain an observed lower limit on the sextet mass of $m_\Phi \approx 2527$ GeV, negligibly different from the expected limit of 2580 GeV. Meanwhile, under the same branching fraction assumptions, we obtain an expected lower limit of $m_\Phi \approx 1417$ GeV and an observed limit of $m_\Phi \approx 1421$ GeV on pair-produced sextets. We display these limits later in Sec. VI; here we simply note that they outstrip the pair-production limits from ATLAS-CONF-2019-040 shown in Fig. 4(b) and are indeed the strongest we can obtain for pair production in any final state with missing energy.

Finally we mention CMS-EXO-17-015 (later CERN-EP-2018-78), a search by the CMS Collaboration for dark matter in events with a leptoquark and missing transverse momentum. The data for this analysis correspond to an integrated luminosity of $\mathcal{L} = 77.4$ fb^{-1}. The basic requirements are an isolated muon with $p_T > 60$ GeV and $E_T^{miss} > 100$ GeV. The leading jet is required to be hard, with $p_T > 100$ GeV, and b-tagged jets are vetoed for reasons similar to ours in the dedicated analysis. Electrons and τ hadron candidates are also vetoed, as are additional muons if they form an opposite-sign muon pair with the leading muon whose invariant mass falls in the window $m_{\mu\mu} = m_Z \pm 10$ GeV. Other than isolation requirements, the final selection requires the transverse mass of the muon and leading jet to exceed 500 GeV.

[5]A light-generation leptoquark pair analysis based on $\mathcal{L} = 139$ fb^{-1} has been released by the ATLAS Collaboration [62], but it treats only the fully visible decays LQ $\to \ell j$.

TABLE IV. Binned yields for (surviving) background processes and the pair of $m_\Phi = 2$ TeV signals following the full selection described in Sec. V. These estimates are computed for $\sqrt{s} = 13$ TeV and $\mathcal{L} = 3$ ab^{-1}. The EFT cutoff is again taken to be $\Lambda = 4$ TeV.

	Lower bound on $m_T(j_1 j_2, E_T^{miss})$ (TeV) (recall that m_T bins are nonoverlapping)																		
Process	0.25	0.50	0.75	1.00	1.25	1.50	1.75	2.00	2.25	2.50	2.75	3.00	3.25	3.50	3.75	4.00	4.25	4.50	4.75
$W+$jets, $W \to \ell\nu$	58.0	58.0	173.9	116.1	347.8	637.6	289.8	173.9	347.8	347.8	58.0	58.0	58.0	58.0	58.0	58.0	58.0	58.0	58.0
Diboson (1ℓ)	0.77	0.77	0.77	0.77	0.77	0.77	1.54	0.77	0.77	0.77	0.38	0.38	0.38	0.38	0.38	0.38	0.38	0.38	0.38
$pp \to \ell\Phi \to \ell\nu jj$	10.6	35.1	101.8	234.5	461.7	684.1	803.4	96.6	47.8	29.0	22.1	17.0	11.1	3.38	3.88	1.46	1.43	0.48	0.99
$pp \to \nu\Phi \to \ell\nu jj$	3.04	4.77	17.0	49.9	75.5	75.3	64.4	39.0	25.3	17.1	8.76	5.25	3.08	1.48	1.34	0.80	0.14	0.41	< 0.1

We apply the MADANALYSIS5 recast of this search to single- and pair-production samples including exactly one muon. The results for single production are displayed in Fig. 10; the pair-production limits are weaker than those from CMS-EXO-17-009 and so we omit them from the discussion.

This figure can be interpreted much like its predecessors: here the theory cross section is in a benchmark with (again) an EFT cutoff of $\Lambda = 4$ TeV and with muon and neutrino branching fractions each set to $\beta = 1/2$. In this benchmark we obtain an observed lower limit on the sextet mass of $m_\Phi \approx 1776$ GeV and an expected limit of 1736 GeV, both of which are weaker than the limits imposed by the CMS search for first-generation leptoquarks in the $e\nu jj$ channel. This discrepancy is despite comparable acceptances of our signal events and the doubling of the dataset for the muon analysis, and is ultimately due to the multi-bin approach of the earlier leptoquark search, which (especially for bins targeting heavier leptoquarks) better suppresses the $W+$ jets and $t\bar{t}$ backgrounds.

VI. LHC SENSITIVITY PROJECTIONS

We finally map the results of Secs. IV and V onto the (m_Φ, Λ) plane and make sensitivity projections for the planned 3 ab^{-1} run of the HL-LHC. This map is displayed in Fig. 11. The custom selection strategy in the mostly visible channel is detailed in Sec. V. Our projections are made using the workflows detailed in Sec. III based on our samples simulated for center-of-mass energy of $\sqrt{s} = 13$ TeV. These sensitivities are therefore conservative in view of upgrades to $\sqrt{s} = 13.6$ TeV or even 14 TeV.

All of the space in Fig. 11 not shaded in gray (due to perturbative unitarity violation; *viz*. Sec. II) is self-consistent EFT parameter space with a promptly decaying color-sextet scalar. The regions shaded in color are excluded by observed limits at 95% CL from one of the searches reinterpreted in the preceding sections. The corresponding expected limits are marked by dashed contours. Our extrapolations to an integrated luminosity of $\mathcal{L} = 3$ ab^{-1} are furthermore marked by thicker solid contours. These limits correspond directly to the benchmarks considered in Secs. IV and V: this

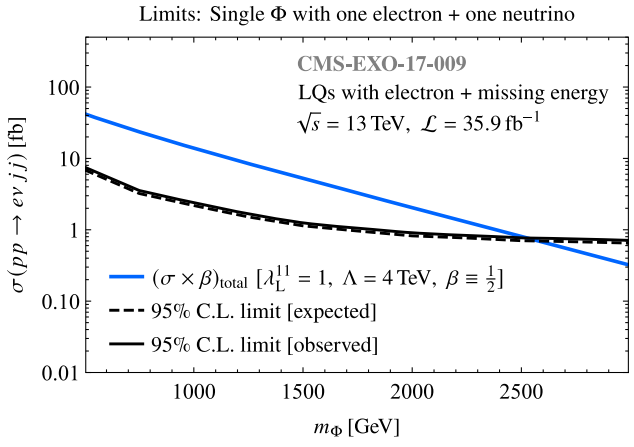

FIG. 9. Observed and expected limits at 95% CL from CMS-EXO-17-009, a Run 2 search for first-generation scalar leptoquarks in final states with jets and either an opposite-sign electron pair or a single electron and missing transverse energy. Only the latter channel applies to this figure. In a scenario with EFT cutoff $\Lambda = 4$ TeV, the observed (expected) lower bound on m_Φ from this search is 2527 (2580) GeV.

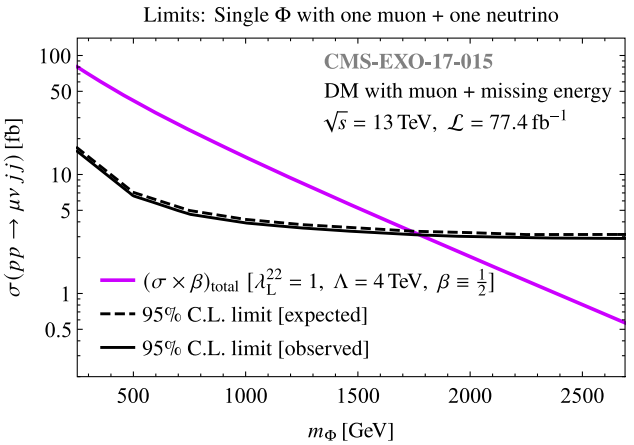

FIG. 10. Observed and expected limits at 95% CL from CMS-EXO-17-015, a Run 2 search for dark matter in events with a muon-philic leptoquark and missing transverse energy. In a scenario with EFT cutoff $\Lambda = 4$ TeV, the observed (expected) lower bound on m_Φ from this search is 1776 (1736) GeV.

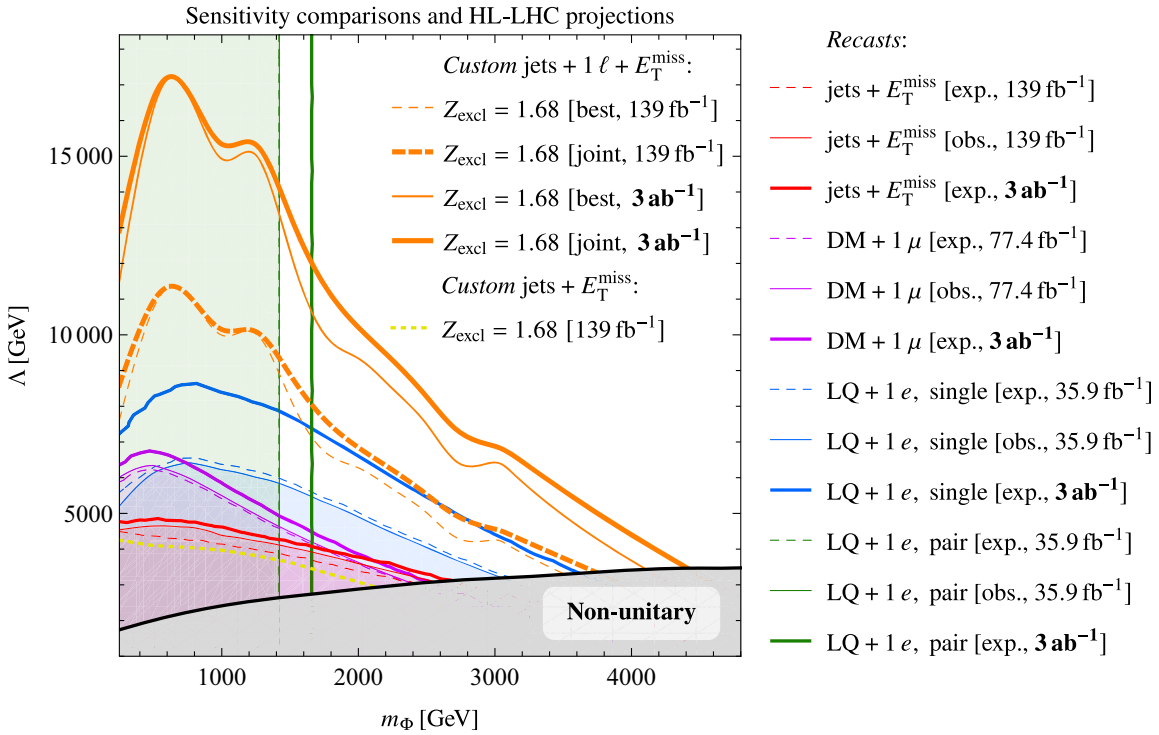

FIG. 11. Map of EFT parameter plane (m_Φ, Λ) showing most recent available Run 2 LHC limits and $\mathcal{L} = 3$ ab^{-1} HL-LHC projected limits, compared to exclusion sensitivity Z_{excl} of our dedicated mostly visible analysis for $\mathcal{L} = 139$ fb^{-1} and 3 ab^{-1}. "Best" limits are derived from most sensitive $m_{\text{T}}(j_1 j_2, E_{\text{T}}^{\text{miss}})$ bin, while "joint" limits use the full m_{T} distribution. Also shown, for reference, is the exclusion sensitivity from the unbinned custom semi-invisible search discussed in Sec. IV.

means that these are the strongest limits than can be derived from each search, since for instance diminishing the sextet branching fraction to electrons would weaken the limits from the CMS search for first-generation leptoquarks. We therefore proceed with the caveat that these limits do not apply simultaneously to any single benchmark scenario.

Figure 11 demonstrates, as discussed earlier, that the CMS search for first-generation leptoquarks (blue) imposes most of the strongest limits on single sextet production in the mostly visible channel. These limits already extend as far as $m_\Phi \approx 3.0$ TeV or $\Lambda \approx 6.2$ TeV, which is even more impressive given the relatively low luminosity of this search. This analysis naturally has the most to gain from additional statistics, such that the projected reach at HL-LHC is as high as $m_\Phi \approx 3.6$ TeV or $\Lambda \approx 8.75$ TeV. For single production, the CMS search for dark matter and a muon is competitive with the LQ analysis for light sextets but rapidly loses sensitivity. The ATLAS jets + $E_{\text{T}}^{\text{miss}}$ search is generally the least sensitive for the reasons discussed in Sec. IV. In the interest of completeness, we include in Fig. 11 the exclusion contour at $\mathcal{L} = 139$ fb^{-1} for our unsuccessful custom jets + $E_{\text{T}}^{\text{miss}}$ analysis detailed in Sec. IV. As mentioned there, we find similar exclusions to the ATLAS-CONF-2019-040 expected limits, but nowhere do we improve upon their results. Moving on, also shown in Fig. 11 are the Λ-independent limits on pair-produced scalars from the CMS leptoquark analysis. As discussed in Sec. IV, just as for single production, the pair-production limits from this search are stronger than those imposed by the other two searches, so we suppress the other sextet pair limits in the interest of visual clarity.

The results of our dedicated analysis in the jets + single lepton + $E_{\text{T}}^{\text{miss}}$ channel are drawn in orange. As in Sec. V, we start with the full Run 2 luminosity of $\mathcal{L} = 139$ fb^{-1} and then extrapolate to $\mathcal{L} = 3$ ab^{-1}. There is a pair of contours for each projection: in each case, the thinner curve traces the values of (m_Φ, Λ) for which the exclusion significance of the most sensitive individual $m_{\text{T}}(j_1 j_2, E_{\text{T}}^{\text{miss}})$ bin attains $Z_{\text{excl}} = 1.68$ ("best"), and the thicker contour ("joint") does the same for the significance computed using the joint likelihood as described in Sec. III. Displaying both contours demonstrates both the power of our custom selections and the additional sensitivity given by considering the full likelihood. We caution once more that these are the most optimistic estimates, since the sensitivity will wane for a real analysis with a full statistical model that includes the correlations between the nonoverlapping m_{T} bins. But we see, at minimum (without the full likelihood), that our analysis is roughly as sensitive with the current LHC dataset as the CMS leptoquark analysis will be after the HL-LHC shuts down. Our analysis moreover outstrips all existing analyses at the HL-LHC, probing singly produced sextets as heavy as $m_\Phi \approx 4.4$ TeV or cutoffs as high as $\Lambda \approx 16.8$ TeV.

VII. CONCLUSIONS

In this work we have compared an array of analyses targeting hard jets and significant missing transverse energy as probes of color-sextet scalar production in association with leptons and/or neutrinos at the LHC. Such processes are minimally allowed by dimension-six operators with a unique $\mathrm{SU}(3)_c$ color structure that has only begun to be explored recently. We have reinterpreted three existing searches within an effective framework to constrain both single and pair production of our sextet scalar. The existing limits are already at the multi-TeV scale for both the sextet mass m_Φ and the cutoff Λ that is related to the scale of ultraviolet physics. Nevertheless, we have demonstrated that the reach of the LHC can be improved by way of a dedicated joint-likelihood analysis, in a channel with one visible lepton, with binned selections of $m_{\mathrm{T}}(j_1 j_2, E_{\mathrm{T}}^{\mathrm{miss}})$, the transverse mass of the two leading jets and missing transverse momentum. Our custom search can ultimately rule out sextet scalars lighter than $m_\Phi \approx 4.4$ TeV or probe cutoffs as high as $\Lambda \approx 16.8$ TeV (14 TeV in space not already excluded for pair production).

It is worthwhile to contrast the limits obtained in this work with the experimental status of color-sextet scalars assumed to couple to the Standard Model through the conventional diquark portal exemplified by (1). Sextets of this class can be directly probed at the LHC with searches for dijet resonances (for single production) and for at least four jets (for pair production), some of which could be b-tagged to target sextets coupling to third-generation quarks. While the limits obtained by recasting such searches are highly sensitive to the couplings (hence branching fractions) of the sextet scalar, direct Run 2 searches have pushed both light-flavor [4,5] and heavy-flavor sextet diquarks [6] to the TeV scale, and in fact above 1.5 TeV for resonances decaying with unit branching fraction to quarks subsequently hadronizing to form flavorless jets. By comparison with Fig. 11, we see that these limits are roughly competitive with, but probably marginally stronger than, the recast limits derived from CMS-EXO-17-009, the search for pair-produced leptoquarks—which we noted are independent of the EFT cutoff Λ. Meanwhile, the diquark couplings of sextet scalars can be probed indirectly by searches for flavor-changing neutral currents in mixings of neutral kaons and D and B mesons, to which sextets can contribute sizably at tree and loop level. The precise bounds depend on whether the sextet couples to up-type, down-type, or mixed quarks; but generally these constraints are very stringent, heavily disfavor democratic couplings to first- and second-generation quarks, and can restrict some dimensionless diquark couplings to be as small as $\mathcal{O}(10^{-6})$ [63].

While we have mentioned these limits to provide context, we caution the reader against viewing these diquark constraints and the results of our work as part of a single coherent picture, and particularly against relating lower bounds on the sextet diquark mass to lower bounds on our EFT cutoff Λ. These two schemes cannot be combined naively because (a) as mentioned in the Introduction, the diquark operators (1) cannot coexist with the effective operators (2) without *at minimum* lepton number violation, and (b) if we suppose that multiple two-body and three-body production/decay channels are available, then it is not clear without a dedicated study what constraints apply to parameter space in which such channels are of comparable size. In the interest of caution, rather, we view the diquark portal and the effective framework as nonoverlapping schemes to be analyzed separately. From this point of view, the interesting lesson of this work and its prequel [9] is therefore that (in appropriately simple benchmark scenarios) the LHC can be used to impose strong limits on resonant sextet scalar production with nonstandard semi-invisible topologies that rival the constraints obtained from conventional multijet searches.

There are a number of other interesting possible extensions of this work. One direction involves applying our EFT results to ultraviolet-complete constructions. It is straightforward to imagine loop-induced couplings of color-charged fields to leptons and neutrinos within existing popular bSM frameworks (featuring, for example, leptoquarks) that might be good candidates for searches like ours that target semivisible three-body decays. Moreover, UV-complete theories may produce nondemocratic sextet branching fractions and more distinct kinematics that could help us further refine the strategy detailed here. An entirely different avenue of study lies in further investigating the jets $+ E_{\mathrm{T}}^{\mathrm{miss}}$ channel, for which crafting a dedicated search with superior sensitivity proved impossible using standard observables. Our sextet model provides an interesting example of a bSM process in the jets $+ E_{\mathrm{T}}^{\mathrm{miss}}$ channel with an asymmetric topology (by which we mean the four-body final state consists of three decay products and a recoiling particle instead of two pairs of two decay products). In principle, this event topology should produce signatures distinct from those of *e.g.* squark pair production. But in this work we were not yet able to surpass the standard jets $+ E_{\mathrm{T}}^{\mathrm{miss}}$ searches designed to target sparticle pair production. We are therefore working on new analyses aimed at exploiting the asymmetric event topology. Sextets are an interesting test case for these signals, but a future analysis would be useful for increasing sensitivity to other bSM scenarios (bino/gluino pair production, to give one example).

We could also explore other novel operators with color sextets. In this work we chose to study $\mathrm{SU}(2)_{\mathrm{L}}$ (weak-) singlet sextets. Other sextet models could contain fields with higher $\mathrm{SU}(2)_{\mathrm{L}}$ representations and would present even more rich phenomenology. We take as inspiration several models, both renormalizable and effective, of color octets with nontrivial $\mathrm{SU}(2)_{\mathrm{L}}$ charge [64–66]. These states can

be fundamentals, adjoints, or even higher multiplets of $SU(2)_L$ [8]. These multiplets contain charged and neutral states and may have various new production modes and subsequently undergo interesting cascade decays [67]. New color-charged states of this class can also have measurable effects on the electroweak precision observables [66]. An immediate possibility is therefore to extend our study of color sextets to include nontrivial $SU(2)_L$ charges and map out some of the most interesting phenomenological consequences.

To take a broader view, new $SU(3)_c$ charged states, with their wide range of new signatures, remain ripe for exploration. New operator catalogs would include interesting diboson production modes and decays [8,65,68] and multiple heavy-flavor events [69]. Following the spirit of this work, we plan to explore other novel EFTs involving exotic color-charged states. Further work with color octets, mentioned above, is one obvious direction. One avenue for further study could be to explore asymmetric single production of exotic color octets in association with other states, as we have done here with sextets.

ACKNOWLEDGMENTS

L. M. C. and K. S. are supported in part by Grant No. DE-SC0024179 from the United States Department of Energy (DOE). T. M. is supported by Grant No. ANR-21-CE31-0013, Project DMwithLLPatLHC, from the *Agence Nationale de la Recherche* (ANR), France.

[1] R. S. Chivukula, M. Golden, and E. H. Simmons, Phys. Lett. B **257**, 403 (1991).
[2] A. Çelikel, M. Kantar, and S. Sultansoy, Phys. Lett. B **443**, 359 (1998).
[3] T. Han, I. Lewis, and T. McElmurry, J. High Energy Phys. 01 (2009) 123.
[4] C.-R. Chen, W. Klemm, V. Rentala, and K. Wang, Phys. Rev. D **79**, 054002 (2009).
[5] T. Han, I. Lewis, and Z. Liu, J. High Energy Phys. 12 (2010) 085.
[6] L. M. Carpenter, T. Murphy, and T. M. P. Tait, J. High Energy Phys. 09 (2022) 175.
[7] L. M. Carpenter, T. Murphy, and T. M. P. Tait, Phys. Rev. D **105**, 035014 (2022).
[8] L. M. Carpenter, T. Murphy, and M. J. Smylie, J. High Energy Phys. 08 (2023) 050.
[9] L. M. Carpenter, T. Murphy, and K. Schwind, Phys. Rev. D **106**, 115006 (2022).
[10] L. M. Carpenter, T. Murphy, and M. J. Smylie, J. High Energy Phys. 11 (2020) 024.
[11] N. Cabibbo, Phys. Rev. Lett. **10**, 531 (1963).
[12] M. Kobayashi and T. Maskawa, Prog. Theor. Phys. **49**, 652 (1973).
[13] N. D. Christensen and C. Duhr, Comput. Phys. Commun. **180**, 1614 (2009).
[14] A. Alloul, N. D. Christensen, C. Degrande, C. Duhr, and B. Fuks, Comput. Phys. Commun. **185**, 2250 (2014).
[15] Wolfram Research, Inc., Mathematica©, Version 12.0 (2020), https://www.wolfram.com/mathematica.
[16] R. Mertig, M. Böhm, and A. Denner, Comput. Phys. Commun. **64**, 345 (1991).
[17] V. Shtabovenko, R. Mertig, and F. Orellana, Comput. Phys. Commun. **207**, 432 (2016).
[18] V. Shtabovenko, R. Mertig, and F. Orellana, Comput. Phys. Commun. **256**, 107478 (2020).
[19] J. Alwall, R. Frederix, S. Frixione, V. Hirschi, F. Maltoni, O. Mattelaer, H.-S. Shao, T. Stelzer, P. Torrielli, and M. Zaro, J. High Energy Phys. 07 (2014), 079.
[20] R. Frederix, S. Frixione, V. Hirschi, D. Pagani, H.-S. Shao, and M. Zaro, J. High Energy Phys. 07 (2018), 185.
[21] C. Degrande, C. Duhr, B. Fuks, D. Grellscheid, O. Mattelaer, and T. Reiter, Comput. Phys. Commun. **183**, 1201 (2012).
[22] D. A. Dicus and V. S. Mathur, Phys. Rev. D **7**, 3111 (1973).
[23] B. W. Lee, C. Quigg, and H. B. Thacker, Phys. Rev. D **16**, 1519 (1977).
[24] T. Cohen, J. Doss, and X. Lu, J. High Energy Phys. 04 (2021) 155.
[25] R. D. Ball, V. Bertone, S. Carrazza *et al.*, Nucl. Phys. **B867**, 244 (2013).
[26] T. Sjöstrand, S. Ask, J. R. Christiansen, R. Corke, N. Desai, P. Ilten, S. Mrenna, S. Prestel, C. O. Rasmussen, and P. Z. Skands, Comput. Phys. Commun. **191**, 159 (2015).
[27] E. Conte, B. Fuks, and G. Serret, Comput. Phys. Commun. **184**, 222 (2013).
[28] E. Conte, B. Dumont, B. Fuks, and C. Wymant, Eur. Phys. J. C **74**, 3103 (2014).
[29] B. Dumont, B. Fuks, S. Kraml, S. Bein, G. Chalons, E. Conte, S. Kulkarni, D. Sengupta, and C. Wymant, Eur. Phys. J. C **75**, 56 (2015).
[30] E. Conte and B. Fuks, Int. J. Mod. Phys. A **33**, 1830027 (2018).
[31] S. Ovyn, X. Rouby, and V. Lemaître, arXiv:0903.2225.
[32] J. de Favereau, C. Delaere, P. Demin, A. Giammanco, V. Lemaître, A. Mertens, and M. Selvaggi, J. High Energy Phys. 02 (2014), 057.
[33] J. Y. Araz, B. Fuks, and G. Polykratis, Eur. Phys. J. C **81**, 329 (2021).
[34] M. Cacciari, G. P. Salam, and G. Soyez, Eur. Phys. J. C **72**, 1896 (2012).
[35] A. L. Read, J. Phys. G **28**, 2693 (2002).
[36] J. Y. Araz, M. Frank, and B. Fuks, Eur. Phys. J. C **80**, 531 (2020).
[37] G. Cowan, K. Cranmer, E. Gross, and O. Vitells, Eur. Phys. J. C **71**, 1554 (2011); **73**, 2501(E) (2013).

[38] Procedure for the LHC Higgs boson search combination in Summer 2011, Technical Report, 2011.
[39] G. Ranucci, Nucl. Instrum. Methods Phys. Res., Sect. A **661**, 77 (2012).
[40] Formulae for estimating significance, Technical Report, 2020.
[41] G. Aad *et al.* (ATLAS Collaboration), J. High Energy Phys. 02 (2020) 143.
[42] K. Melnikov and F. Petriello, Phys. Rev. D **74**, 114017 (2006).
[43] R. Gavin, Y. Li, F. Petriello, and S. Quackenbush, Comput. Phys. Commun. **182**, 2388 (2011).
[44] Y. Li and F. Petriello, Phys. Rev. D **86**, 094034 (2012).
[45] Multi-boson simulation for 13 TeV ATLAS analyses, Technical Report No., ATL-PHYS-PUB-2016-002, CERN, Geneva, 2016.
[46] T. Gleisberg, S. Hoeche, F. Krauss, M. Schonherr, S. Schumann, F. Siegert, and J. Winter, J. High Energy Phys. 02 (2008) 007.
[47] M. Czakon and A. Mitov, Comput. Phys. Commun. **185**, 2930 (2014).
[48] J. M. Campbell and R. K. Ellis, J. High Energy Phys. 07 (2012) 052.
[49] J. Campbell, T. Neumann, and Z. Sullivan, J. High Energy Phys. 02 (2020) 040.
[50] R. D. Ball *et al.* (PDF4LHC Working Group), J. Phys. G **49**, 080501 (2022).
[51] N. Kidonakis and N. Yamanaka, J. High Energy Phys. 05 (2021) 278.
[52] M. L. Mangano, M. Moretti, F. Piccinini, and M. Treccani, J. High Energy Phys. 01 (2006) 013.
[53] R. D. Ball *et al.* (NNPDF Collaboration), J. High Energy Phys. 04 (2015) 040.
[54] P. Nason, J. High Energy Phys. 11 (2004) 040.
[55] S. Frixione, P. Nason, and C. Oleari, J. High Energy Phys. 11 (2007) 070.
[56] S. Alioli, P. Nason, C. Oleari, and E. Re, J. High Energy Phys. 06 (2010) 043.
[57] H.-L. Lai, M. Guzzi, J. Huston, Z. Li, P. M. Nadolsky, J. Pumplin, and C. P. Yuan, Phys. Rev. D **82**, 074024 (2010).
[58] J. M. Campbell and R. K. Ellis, Nucl. Phys. B, Proc. Suppl. **205–206**, 10 (2010).
[59] S. Dulat, T.-J. Hou, J. Gao, M. Guzzi, J. Huston, P. Nadolsky, J. Pumplin, C. Schmidt, D. Stump, and C. P. Yuan, Phys. Rev. D **93**, 033006 (2016).
[60] R. D. Ball *et al.* (NNPDF Collaboration), Eur. Phys. J. C **77**, 663 (2017).
[61] A. M. Sirunyan *et al.* (CMS Collaboration), Phys. Rev. D **99**, 052002 (2019).
[62] G. Aad *et al.* (ATLAS Collaboration), J. High Energy Phys. 10 (2020) 112.
[63] K. S. Babu, P. S. Bhupal Dev, E. C. F. S. Fortes, and R. N. Mohapatra, Phys. Rev. D **87**, 115019 (2013).
[64] A. V. Manohar and M. B. Wise, Phys. Rev. D **74**, 035009 (2006).
[65] L. M. Carpenter, M. J. Smylie, J. M. C. Ramirez, C. McDowell, and D. Whiteson, Phys. Rev. D **105**, 075027 (2022).
[66] L. M. Carpenter, T. Murphy, and M. J. Smylie, Phys. Rev. D **106**, 055005 (2022).
[67] L. M. Carpenter and S. Mantry, Phys. Lett. B **703**, 479 (2011).
[68] L. M. Carpenter and R. Colburn, J. High Energy Phys. 12 (2015) 151.
[69] L. M. Carpenter, T. Murphy, and M. J. Smylie, J. High Energy Phys. 01 (2022) 047.